MICROSTRUCTURAL AND THERMAL CONDUCTIVITY INVESTIGATION OF THERMAL BARRIER COATINGS BY ELECTRON BEAM-PHYSICAL VAPOR DEPOSITION OF ZIRCONIA CO-DOPED WITH YTTRIA AND NIOBIA[1]

Daniel Soares de Almeida [2]
Carlos Alberto Alves Cairo[2]
Maria do Carmo Andrade Nono[3]
Cosme Roberto Moreira da Silva [4]

Abstract
The most usual ceramic material for coating turbine blades is yttria doped zirconia. Addition of niobia, as a co-dopant in the Y_2O_3-ZrO_2 system, can reduce the thermal conductivity and improve mechanical properties of the coating. The purpose of this work is to evaluate the influence of the addition of niobia on the microstructure and thermal properties of the ceramic coatings. SEM on coatings fractured cross-section shows a columnar structure and the results of XRD show only zirconia tetragonal phase in the ceramic coating for the chemical composition range studied. As the difference $NbO_{2,5}$-$YO_{1,5}$ mol percent increases, the tetragonality increases. A significant reduction of the thermal conductivity, measured by laser flash technique, in the zirconia coating co-doped with yttria and niobia when compared with zirconia-yttria coating was observed.
Key words: TBC, EB-PVD, Zirconia, Niobia, Thermal Conductivity.

INVESTIGAÇÃO DA MICROESTRUTURA E DA CONDUTIVIDADE TÉRMICA DE REVESTIMENTOS DE ZIRÔNIAS CO-DOPADAS COM ÍTRIA E NIÓBIA COMO FORMA DE BARREIRA TÉRMICA OBTIDOS POR DEPOSIÇÃO FÍSICA DE VAPORES POR FEIXE DE ELÉTRONS

Resumo
O material cerâmico mais utilizado para revestimentos de palhetas de turbine é a zircônia dopada com ítria. A adição de nióbia com co-dopante no sistema Y_2O_3-ZrO_2 pode reduzir a condutividade térmica e melhorar as propriedades mecânicas de tais revestimentos. O objetivo deste trabalho é avaliar a influência da adição de nióbia na microestrutura e propriedades térmicas dos revestimentos cerâmicos. Análises por MEV na superfície de fratura da seção transversal destes revestimentos mostrou uma estrutura colunar e os resultados de difração de raios X mostrou apenas a fase tetragonal nos revestimentos nas composições químicas estudadas. À medida que a diferença $NbO_{2,5}$-$YO_{1,5}$ % mol aumenta, a tetragonalidade aumenta. Foi observada uma significativa redução da condutividade térmica, medida pela técnica “laser flash”, nos revestimentos de zircônia co-dopada com ítria e nióbia quando comparada com os revestimentos de zircônia dopada com ítria.
Palavras-chave: TBC, EB-PVD, Zircônia, Nióbia, Condutividade Térmica.

[1] *Technical Contribution to the 63 National Congress of the ABM, Jully 28th 2007, Santos – SP – Brazil.*
[2] *Comando-Geral de Tecnologia Aeroespacial, São Jose dos Campos, SP*
[3] *Instituto Nacional de Pesquisas Espaciais, São Jose dos Campos, SP*
[4] *Universidade Federal de Brasília*

1 INTRODUCTION

The great advantage of coatings is that it is possible to modify its response to the environment by changing only the superficial part of the component, thus providing completely different properties. Some of the obtained benefits are: reduction of maintenance costs, increase of the working temperature, reduction of thermal loads, resistance increase to erosion and corrosion and reduction of the high temperature oxidation[1].
The electron beam-physical vapor deposition (EB-PVD) process enables to attain coatings with unique properties. The process parameters are adjusted so that the deposit has a columnar grain structure perpendicular to the interface. This morphology maximizes the resistance to strains that arise from differences in thermal expansion coefficients. Other advantages are: aerodynamically favorable smooth surface, better interaction with the substrate, greater thermal cycle tolerance and, hence, greater lifetime comparativeness with the plasma spray process [2-13].
There are four primary constituents in a thermal protection system. They comprise: (1) the thermal barrier coating (TBC) itself based usually on ~ 8 wt. % (8.7 mol % $YO_{1.5}$) yttria stabilized zirconia; (2) the metallic component, treated here as the substrate; (3) an aluminium containing bond coat (BC) located between the substrate and the TBC; and (4) a thermally grown oxide (TGO), predominantly α-alumina, that forms between the TBC and the bond coat. The TBC is the thermal insulator, the bond coat provides oxidation protection, since the zirconia is essentially transparent for the oxygen at high temperatures, and the metallic component, usually a nickel base super-alloy, sustains the structural loads. The TGO is an oxidation reaction product of the bond layer, and plays a role in the metal/oxide adhesion. Each of these elements is dynamic and all interact to control the performance and durability [14,15].

When ZrO2 is utilized for technical applications the high-temperature polymorphs cubic (c) and tetragonal (t) phases should be stabilized at room temperature by the formation of solid solutions, which prevent deleterious tetragonal-to-monoclinic (m) phase transformation. The alloying oxides, which lead to the stabilization, are alkaline-earth, rare-earth, and actinide oxides. It has been suggested that the factors, which may influence the stabilization, are size, valency, and concentration of solute cations and crystal structure of the solute oxides, where the valency and concentration determine the number of oxygen vacancies created by the formation of substitutional solid solutions [16,17].
Dense zirconia based materials already exhibit low thermal conductivity. The introduction of a stabilizer, required to avoid the detrimental effect of tetragonal to monoclinic phase transformation, is accompanied by the incorporation of a substantial amount of vacancies providing an efficient source of phonons scattering [3]. When a trivalent oxide, e.g., Y_2O_3, is added to ZrO_2 as a stabilizer, a certain amount of lattice defects, e.g., oxygen vacancies and negatively charged solutes, are produced in the ZrO_2 lattice [18].
The addition of Ta_2O_5, Nb_2O_5 and HfO_2 to bulk Y_2O_3–stabilized tetragonal ZrO_2 increases transformation, as for example the tetragonal (t) to monoclinic (m) transformation temperature, of the resulting zirconia ceramics. The enhanced transformability is related to the alloying effect on the tetragonality (*c*/*a*—cell parameters

ratio) of stabilized tetragonal ZrO_2 (Fig.1), subsequently, by adding these oxides the tetragonal distortion of the cubic lattice is increased. The increase in the tetragonality, due to alloying, is consistent with the increase in the fracture hardness and the increase in the t to m transformation temperature [13, 19-22]. Evidently, t-ZrO_2 become unstable as their tetragonality increases toward 1.020, which corresponds to the c/b axial ratio of m-ZrO_2 at room temperature. On the other hand, they become stable as the tetragonality decreases toward unity, which corresponds to c-ZrO_2. This relationship allows the classification of oxides into either a stabilizer (decreasing tetragonality) or a destabilizer (increasing tetragonality) for the t-ZrO_2 phase [16, 18, 23].

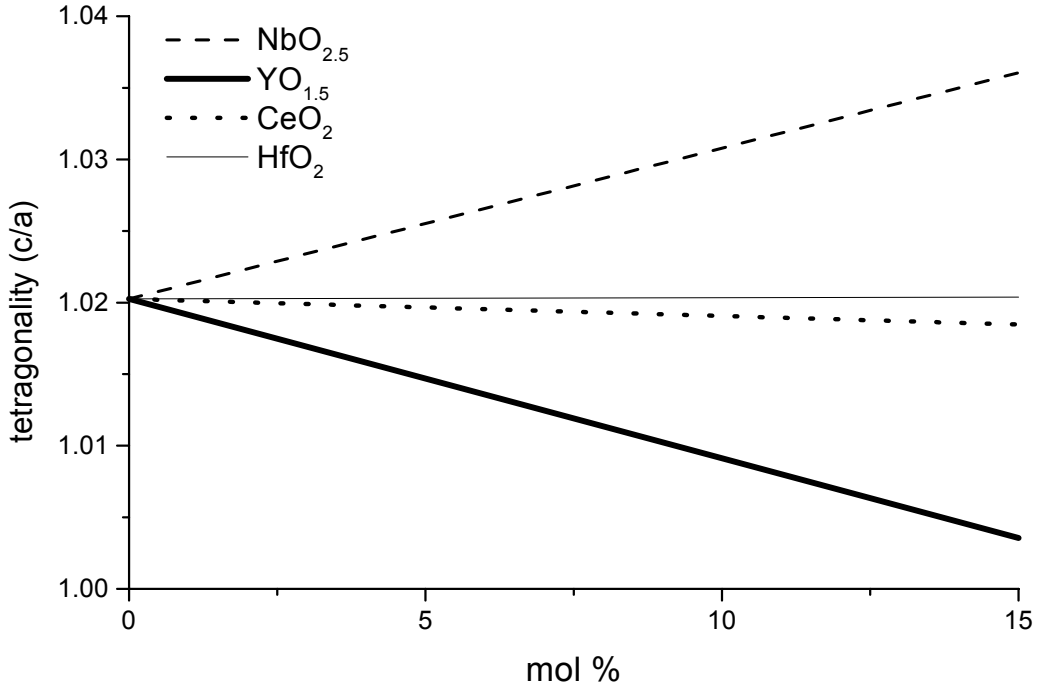

Fig. 1: Influence of the alloying oxide in the c/a axial ratio of bulk zirconia based ceramics.

The thermal conductivity of partially stabilized-ZrO_2 (PSZ) is determined by its defect structure and the association between defects. Contrary to trivalent oxides, pentavalent oxides are positively charged when dissolved in the ZrO_2 lattice, the addition of these oxides in the partially stabilized zirconia (PSZ) will definitely affect the original defect structure, thus also its properties [13]. The effect of doping with pentavalent oxides, such as tantala and niobia (cationic radii in the +5 oxidation state ~ 0.68 Å for both), indicate that both ions reside as substitutional defects in the zirconium lattice (ionic radius of the Zr^{4+} ion is 0.79 Å), annihilating oxygen vacancies generated by yttria doping. Thus, the defects generated by the two dopants is also identical and would be expected to scatter phonons, i.e. can reduce the thermal conductivity, due to the difference in ionic radius and atomic bonding [19].
Thermal conductivity is one of the physical key properties of the TBCs and, increasing its insulation capability emerges as a technical and economical challenge for engine

manufacturers. Lowering TBCs thermal conductivity would increase the engine performance by improving the combustion efficiency (higher turbine entry temperature), reduce the specific fuel consumption, allow for reduction of internal cooling, reduce the metallic component temperature and extend their lifetime [9, 16, 18, 21, 23].
The thermal conductivity, k, of ceramic coatings can be measured using either a direct (steady state) or a transient approach. In the latter, the thermal diffusivity, α, of a material is measured and subsequently related to thermal conductivity using the relationship:

$$k = \alpha c_p \rho \quad (1)$$

where cp is the heat capacity at constant pressure and ρ is the specific mass of the material.
There are several classical techniques to measure the thermal properties of a material. Such classical methods, which involved the fitting of steady state and non-steady state experimental temperature data to theoretical models, were usually time expendable. Furthermore, the large sized samples imposed intolerable limitations, usually tied to heat losses and contact resistance between the specimen, and its associated heat source, heat sinks and measurement devices. The flash method, used in the present work, eliminated the problem of contact resistance and minimized heat losses by establishing the measuring time to be sufficiently brief so that very little cooling could take place [24, 25].
The study of the considered ceramic coating is motivated by the potential of the niobia to overcome the deficiencies presented in conventional yttria stabilized zirconia coatings, i.e. high thermal conductivity when compared with plasma spray coatings and relatively low mechanical properties.

2 EXPERIMENTAL

SAE 304 stainless steel plates were used as metallic substrates. Both bond layer and ceramic top coating were EB-PVD deposited using one source 30kW electron beam equipment. This consists of an electron gun with accelerating voltage of 25 kV and beam current variation from 0 to 1.2 A. The vacuum system has an ultimate pressure of 10^{-6} torr (~ 10^{-4} Pa). A substrate holder assembly is situated above the vapor source at a vertical distance of 150 mm. A tungsten filament is used to heat the substrate by Joule effect to the desired temperature (~500 ^{o}C) during bond coating deposition and ~900 ^{o}C during ceramic layer deposition), which is measured and maintained by a thermocouple and programmable temperature controller. A water-cooled copper crucible is used for evaporation of sintered targets. The ceramic targets (cylinders of 20mm diameter and mass of 20 g) were prepared from cold compacted powder mixtures of zirconia, yttria and niobia sintered at 1700 ^{o}C under vacuum (10^{-4} Pa). The MCrAlY targets were prepared from a Ni–31Cr–11Al–0.65Y (wt %) powder alloy sintered at 1340 ^{o}C under vacuum (10^{-4} Pa). The bond layer has a thickness of 25 μm.
The crystalline phases of ceramic coatings, with an average thickness of 50 μm, are identified by X-ray diffraction using a X'Pert Philips PW 1380/80 diffractometer and a X'Pert – MRD Philips diffractometer with a PW 3050 goniometer. The ceramic coating microstructure and grain morphology were observed by SEM and the chemical composition was estimated by EDS using a LEO 435 VPI scanning electron microscope.

The specific mass (ρ), disregarding pores and other defects, was calculated from the cell parameters (from XRD data) and molar concentrations of zirconia, yttria and niobia (from EDS analysis), using the equation:

$$\rho = \frac{n.[x.A_{YO1,5} + y.A_{NbO\ 2,5} + (1-x-y).A_{ZrO\ 2}]}{6{,}02\ .10^{23}.a^2.c} \quad (2)$$

where: n – cations in unit cell (n=4 for fcc); $A_{YO1.5}$ – yttria atomic mass (112.905); $A_{NbO2.5}$ – niobia atomic mass (132.905); A_{ZrO2} – zirconia atomic mass (123.22); x and y – molar fraction of yttria and niobia, respectively; a and c – cell parameters of t-ZrO_2 calculated from XRD data.

For thermal properties determinations of coatings the Thermal Flash 2000/Holometrix equipment was used. This method, laser technique, consists of heating the front surface of a thermally insulated specimen with a high-intensity short-duration radiative heat pulse and measuring the temperature evolution on the back surface by means of an infrared detector. The non-intrusive backside measurement method eliminates the concern and issues with sensor attachment to the sample, and removes all uncertainties associated with contact resistance and sensor measurement accuracy [24]. After the sample has been stabilized at a desired uniform temperature (T_0), a nearly instantaneous pulse of energy (usually laser, Xenon lamp or other discharge source) is imposed on its front surface, as well as on the temperature increase on the rear surface of the sample and is then recorded as a function of time. The thermal diffusivity is then determined by comparing this thermogram with theoretical models that describe this transient heat conduction phenomenon. Several theoretical models are available for the flash method, which include adiabatic boundary conditions, heat losses, surface coating effects, among many other aspects. The values of thermal diffusivity (average of three measurements, for each sample at each temperature) was calculated in accordance with the Degiovaninni model [25]. Considering that the energy of the laser is used only for heating the sample, disregarding the interfaces (contact resistance) and using Eq. (3) it is possible to calculate the coating thermal conductivity from Holometrix equipment measurements.

$$\left(\frac{e_a{}^2}{\alpha_a}\right) = \left(\frac{e_m^2}{\alpha_m}\right)\left[1 + \frac{\rho_c c_c e_c}{\rho_m c_m e_m}\left(1 + \frac{3}{2}\frac{e_c/k_c}{e_m/k_m}\right)\right]^2 \quad (3)$$

Where *c* is the heat capacity (J/kgK), ρ is the specific mass (g/cm^3), α is the thermal diffusivity (cm^2/s), k is the thermal conductivity (W/mK), *e* is the thickness (m) and the index *a*, *m* and *c* is relative to the sample, metallic substrate and ceramic layer, respectively.

3 RESULTS AND DISCUSSION

Typical microstructure of EB–PVD coating, as seen by scanning electron microscopy on fractured cross-section, is shown in Fig. 2. It is possible to see the ceramic layers where the columnar structure is evident. Measurements on ceramic coatings fractured cross-section show almost the same size of columns diameter for samples 1 and 6 (Table 1), without significant differences in the columns morphology. However, for sample 11, were the amount of niobia is higher the columns diameter was increased.

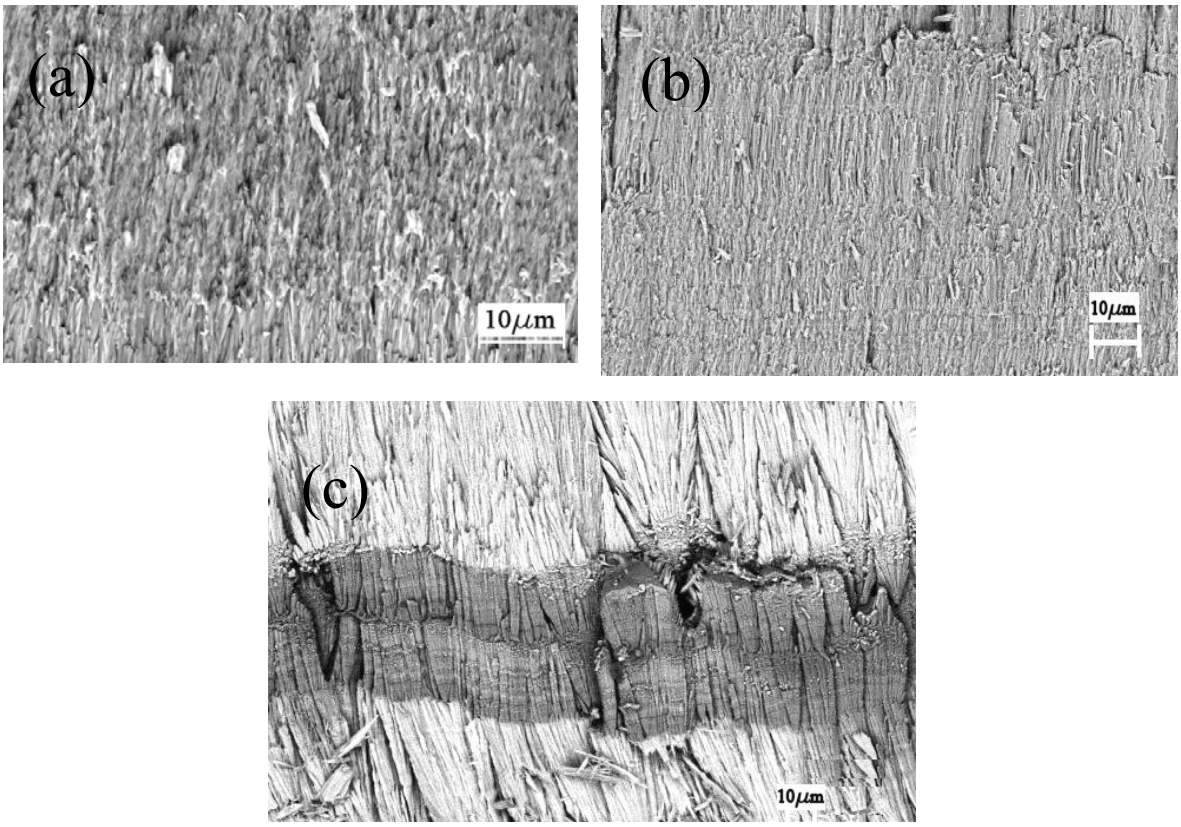

Fig. 2: SEM of EB–PVD ceramic coatings fractured cross-section. (a) Sample 1 (column diameter=1.15 μm), (b) Sample 6 (column diameter=1.29 μm), (c) Sample 11 (column diameter=2.53 μm).

X-ray diffractions with high angular resolution (0,0001^{o} for 2θ) performed on the ceramic coating samples surface with different niobia contents show only the zirconia tetragonal phase. XRD techniques do not allow the identification of special textures related to XRD peak intensity because the PVD coatings show a strong crystallographic texture and the diffraction patterns are taken normal to the substrate surface, not in the coating primary growth direction [26]. However, the X-ray diffraction technique allow determining, with sufficient precision, the position of the peaks. The position of the peaks is correlated with crystalline cell lattice parameters and these vary strongly with the chemical composition of the films.

The chemical composition, the cell parameters deduced from diffraction patterns and the values of specific mass of the coatings are reproduced in Table 1.

Fig. 3 shows the influence of the difference ($NbO_{2.5}$–$YO_{1.5}$) mol% on the zirconia tetragonality. The tetragonality was calculated from the (111) and the (400) peaks position of the XRD diffractograms on the surface of the zirconia based coatings. Chemical composition was determined by EDS analysis on the ceramic coating cross-section. As the difference ($NbO_{2.5}$–$YO_{1.5}$) mol% increases, the ratio c/a (tetragonality) increases. Despite the compositional gradients in the coatings and inaccuracy of oxide semiquantitative analyses by EDS techniques, linear regression shows a high linear coefficient (R =0.920).

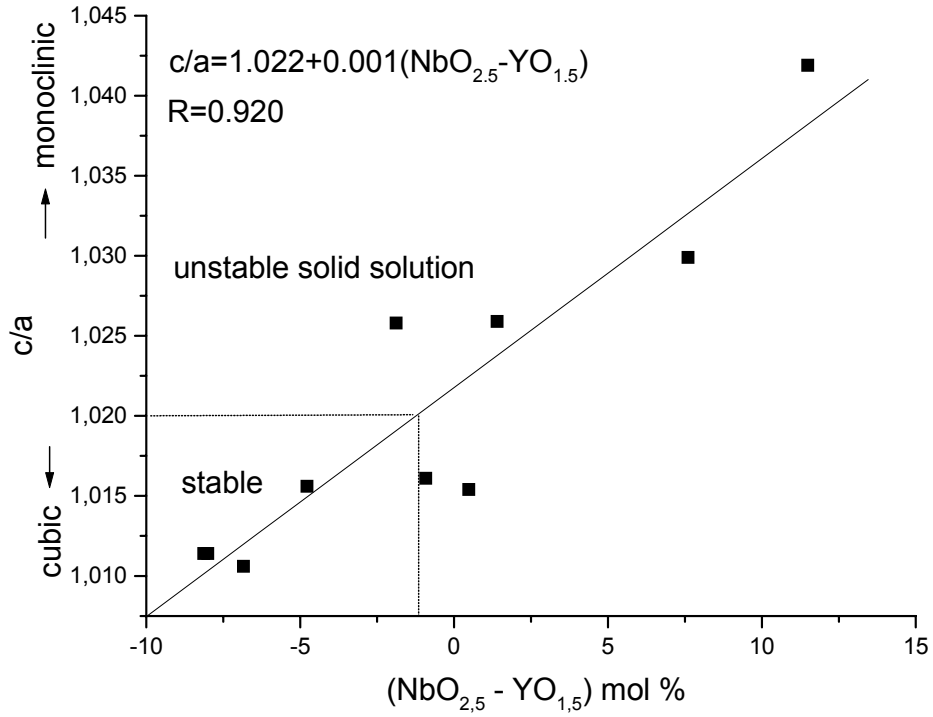

Fig. 3: Relation between difference ($NbO_{2.5}$ -$YO_{1.5}$) mol % and tetragonality (c/a).

Research with sintered tablets (bulk material) of stabilized tetragonal ZrO_2 show they become unstable as their tetragonality increases toward 1.020, at room temperature [9, 18]. This research agrees with the present work experimental results where niobia–yttria–zirconia coatings with $NbO_{2.5}$ contenting higher than 7 mol% (c/a >1.020) had a tendency to spall after the deposition cycle. It is possible to evaluate the maximum content of niobia that can be added to the yttria doped zirconia coating without losses in its mechanical properties. Thus, through the graph of Fig. 3, a coating with 8.7 mol% $YO_{1.5}$ (8 wt.% yttria) can be co-doped with up to 10 mol% $NbO_{2.5}$ (10.8 wt.% niobia).
Fig. 4 shows the typical microstructure of EB–PVD ceramic coating, as seen by SEM on polished cross-section. The ceramic layer shows color bands associated with chemical composition changes due to the differences in saturation vapor pressure of the individual components as function of the temperature and complex chemical inter actions between them. For these reasons, the evaporation of alloys is a selective process, resulting in depletion and enrichment in the melt pool and, consequently, in the coating.

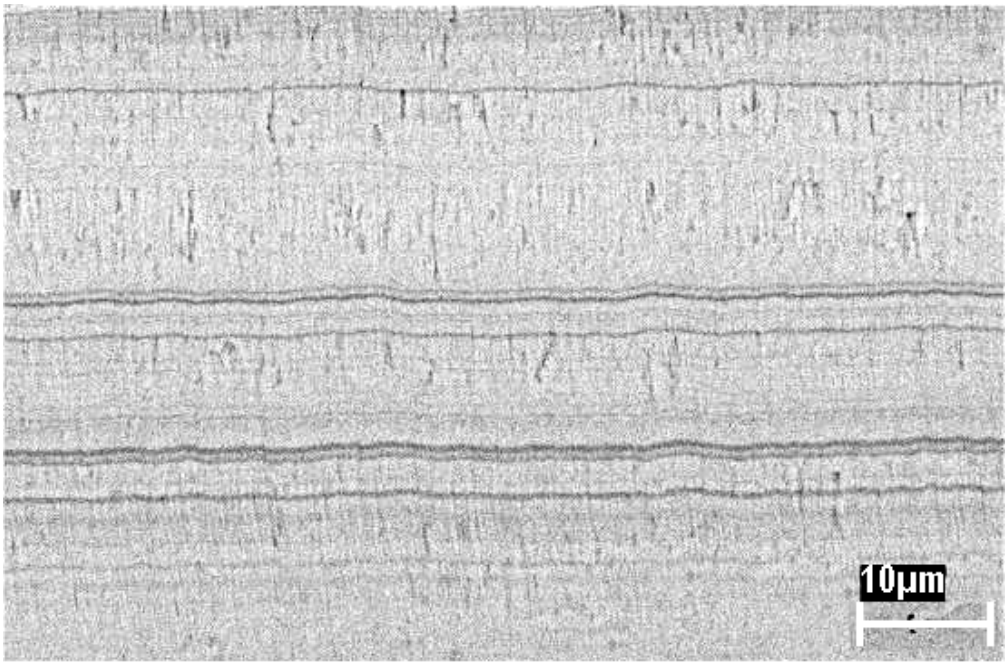

Fig. 4: SEM (BS mode) of an EB-PVD ceramic coating polished cross section (sample 3).

The results of EDS analysis performed on the ceramic coating cross-section are summarized in Fig. 5. The composition of the ceramic layer differs point-to-point, remarkable for the niobia concentration, due to the difference in melting point and vapor pressure between niobia, zirconia and yttria. It is clear that compositional gradients can reduce the thermal stability due to differences in layers thermal expansion coefficients. Nevertheless, because of the high melting point of the ceramic, the liquid pool during evaporation is shallow in comparison with target volume, there is not sufficient liquid volume for high level of segregation and as the process is predominantly random, the influence on the thermal stability and in the X-ray data is not high.

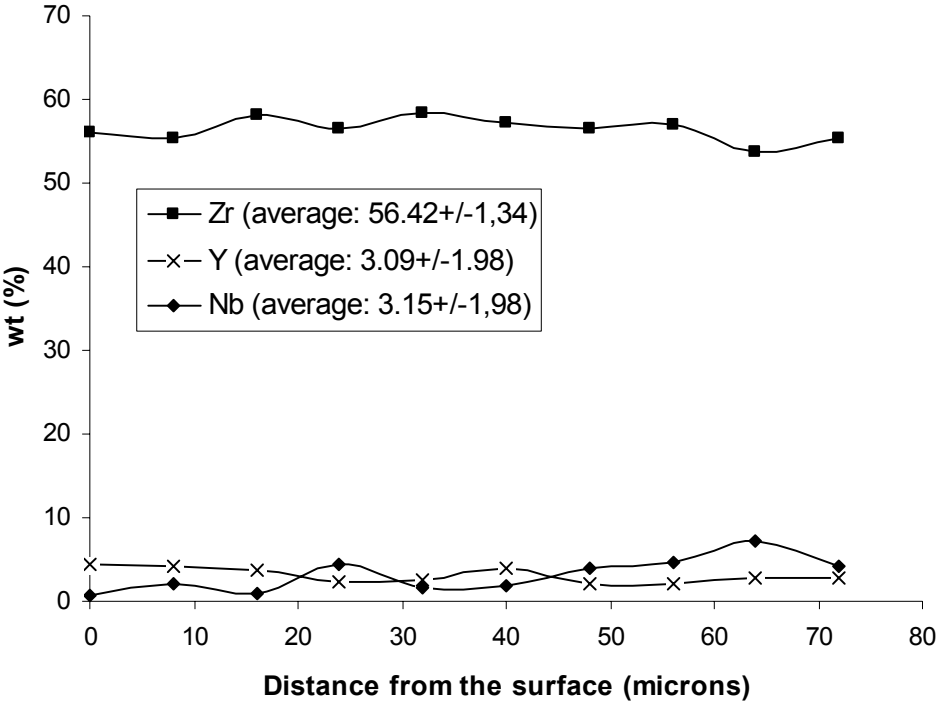

Fig. 5: EDS semi-quantitative analysis of ceramic layer (sample 11).

Another factor that reduces the influence of the multilayer nature of the coatings with differences in composition between the layers in the XRD data is the X-ray penetration (attenuation length) [27]. ZrO2 has an attenuation length of 17 μm (phonon energy of 8050 eV and incident angle of 90°) thus; the XRD data is based on integration or average of a significative thickness of the coatings.

Two ceramic formulation coating samples (sample 12 and 13, table 1) were used for determination of the coatings thermal conductivity. The measurements of thermal diffusivity samples are carried out on coatings with their substrates and bond coats attached to them. All samples were coated with colloidal graphite to optimize the laser energy absorption (black body) and to uniformize infrared sensor data acquisition in the sample backside during thermal diffusivity measurements. On account of its high thermal conductivity value in comparison with zirconia ($k_{graphite}$ = 24 W/m K, $k_{zirconia}$ = 1 W/m K, at 25 ° C), the graphite layer (thickness of ~30μm) was not considered in the calculations.

Figure 6 presents the coatings thermal conductivity variation with the temperature as calculate by using Eq. (3). The zirconia heat capacity values were taken from literature [21], this approach is possible due to the little influence of the oxides dopants in this zirconia physical properties. Thermal conductivity of standard 6–8 wt.% yttria partially stabilized zirconia EB-PVD coatings is typically 1.5–1.9 W/m K. The thermal conductivity of a ceramic layer depends on the intrinsic thermal conductivity of the bulk ceramic, which is linked with its composition and structure, and with the framework of the porous structure, i.e. pore volume fraction, geometry and distribution [3, 28].

Table1: Chemical composition and lattice parameters of the samples

Sample	mol %*$YO_{1.5}$	mol %* $NbO_{2.5}$	Cell parameters a	c	c/a	ρ
1	8.00	0	5.1070	5.1650	1.0114	6.04
2	8.13	0	5.1040	5.1620	1.0114	6.05
3	6.84	0	5.0950	5.1490	1.0106	6.09
4	4.78	0	5.1170	5.1970	1.0156	6.00
5	5.13	5.10	-	-	-	-
6	6.12	7.52	5.1000	5.2320	1.0259	6.02
7	10.67	8.79	5.0840	5.2150	1.0258	6.06
8	10.37	10.85	5.1240	5.2030	1.0154	6.00
9	13.79	12.87	5.0960	5.1780	1.0161	6.10
10	8.53	20.02	5.1050	5.3190	1.0419	5.99
11	10.40	14.50	5.1240	5.2770	1.0299	5.93
12	8.7	0	5.096	5.165	1.0135	6.06
13	8.7	5.6	5.100	5.212	1.0220	6.02

*From EDS analysis on ceramic coating cross section.

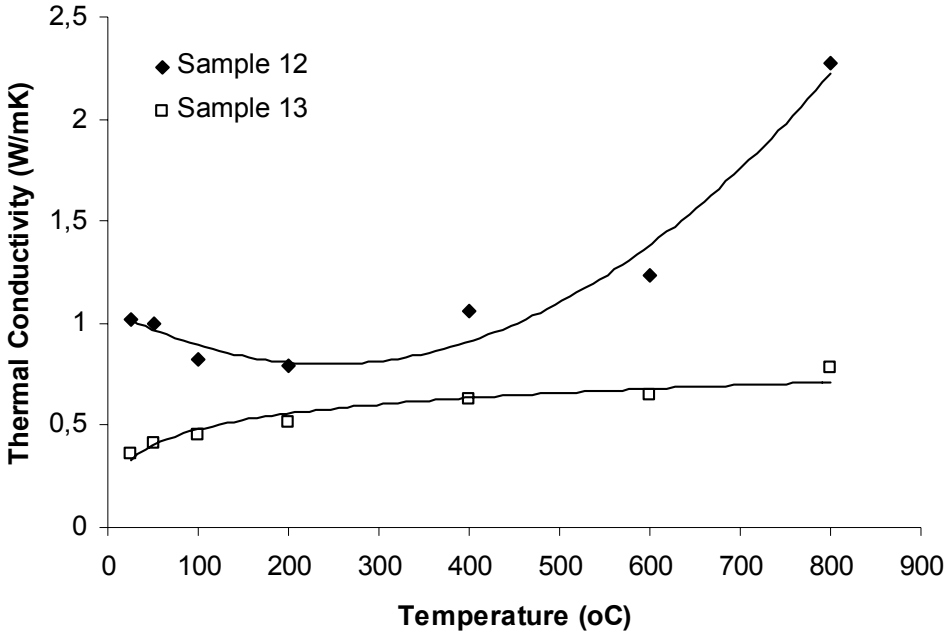

Fig. 6: Variations of coatings thermal conductivity with temperature.

The present work shows an yttria doped zirconia coating, with mean thermal conductivity value of 1.17 W/m K, significantly lower to those indicated by literature for EB-PVD coatings (1.5–1.9 W/m K). This reduction can be explained by the coating thickness. The thermal conductivity of EB-PVD PYSZ coatings strongly depends on the coating thickness with lower values for thin TBCs, this effect is caused by the different microstructure across the coating roughly characterized by a fine grained inner zone and a coarse grained outer zone [29]. A 50% reduction in the yttria niobia co-doped zirconia coating thermal conductivity (average value: 0.54 W/m K) was observed when compared with yttria doped zirconia coating.
Schulz et al. [28] developed a model based on solid state physics considerations regarding heat conduction mechanisms in disordered oxide ceramics for the calculation of the thermal conductivity of zirconia based materials doped with trivalent ions and co-doped with pentavalent metallic ions, showing that significant decrease in thermal conductivity (up to 40%) can be achieved, when compared to the standard 8 wt.% yttria partially stabilized zirconia.
The reduction of almost 50% in the thermal conductivity coating promoted by niobia addition can be attributed to several factors: the increase in the level of porosity of the yttria niobia co-doped zirconia coating; the phonons scattering promoted by the ionic radii differences and chemical bonds between matrix (zirconia) and dopants (niobia and yttria), and, in lesser degree, to the small reduction of the specific mass coating promoted by the niobia addition.

4 CONCLUSIONS

The niobia addition, up to 6 wt.%, as co-dopant in the yttria partially stabilized zirconia coatings is insufficient to change its microstructure.
The laser flash technique in conjunction with Degiovaninni model demonstrates efficiency to determine thermal conductivity of the TBC attached to the substrates.
The single-phase tetragonal niobia and yttria co-doped zirconia coatings show a lower thermal conductivity than conventional 6–8 mol% yttria stabilized zirconia coating, the material conventionally used for thermal barrier coating.

ACKNOWLEDGMENT

The authors express their gratitude to FAPESP (process number: 02/06514-1) and CNPq (process number: 490845/2006-1) for financial support.

REFERENCES

1. K. Funatani, Surf. Coat. Technol. 133–134 (2000) 264–272.
2. H. Xu, S. Goug, L. Deng, Thin Solid Films 334 (1998) 98–102.
3. U. Schulz, et al., Surf. Coat. Technol. 133–134 (2000) 40–48.
4. A.G. Evans, et al., Prog. Mater. Sci. 46 (2001) 249–271..
5. D. Zhu, et al., NASA/TM-2000-210238
6. G.W. Goward, Surf. Coat. Technol. 108–109 (1998) 73–79.
7. J.R. Nicholls, M.J. Deakin, D.S. Rickerby, Wear 233–235 (1999) 352– 361.
8. N. Czek, et al., Surf. Coat. Technol. 113 (1999) 157–164.

9. D.D. Hass, Doctor Degree Thesis, University of Virginia, May 2001.
10. D.S. Almeida, et al., Mater. Sci. And Engineering A 443 (2007) 60-65.
11. D.S. Almeida, et al., Surf. Coat. Technol. 200 (2006) 2827-2833.
12. J.R. Nicholls, et al., Surf. Coat. Technol. 151–152 (2002) 383–391.
13. X. Guo, J.Z. Wang, Eur. Ceram. Soc. 18 (1998) 237–240.
14. D.R. Mumm, A.G. Evans, I.T. Spitsberg, Acta Mater. 49 (2001) 2329.
15. D. Stöver, C. Funke, J. Mater. Process. Technol. 92–93 (1999) 195.
16. D.J. Kim, J. Am. Ceram. Soc. 73 (1) (1990) 115.
17. H. Lehmann, et al., J. Am. Ceram. Soc. (8) (2003) 1138.
18. D.J. Kim, T.Y. Tien, J. Am. Ceram. Soc. 74 (12) (1991) 3061.
19. S. Raghavan, et al., Acta Mater. 49 (2001) 169–179.
20. H. Guo, X. Bi, S. Gong, H. Xu, Scripta Mater. 44 (2001) 683–687.
21. S. Raghavan, et al., Scripta Mater. 39 (8) (1998) 1119–1125.
22. D.J. Kim, J. Am. Ceram. Soc. 73 (1) (1990) 115–120.
23. D.Y. Lee, et al., J. Mater. Sci. Lett. 17 (1998) 185.
24. P. Couto, et al., Metrologia-2003, Anais. Recife, Pernambuco, Brasil, 2003.
25. A. Degiovaninni, M. Lament, Rev. Phys. Appl. 21 (1986) 229–237.
26. J.S. Bernier, et al., Surf. Coat. Technol. 95–99 (2003) 163.
27. B.L. Henke, et al., At. Data Nucl. Data Tables 54 (2) (1993) 181.
28. U. Schulz, et al., Aerospace Sci. Technol. 7 (2003) 73–80.
29. H.-J. Rätzer-Scheibe, et al, Surf. Coat. Technol. 200 (2006) 5636-5644.